$\mathcal{R}$esearch in
$\mathcal{A}$stronomy and
$\mathcal{A}$strophysics

A catalogue of Hα emission-line point sources in the vicinity fields of M 31 and M 33 from the LAMOST survey

Meng Zhang (张萌)[1,2,3], Bing-Qiu Chen (陈丙秋)[2], Zhi-Ying Huo (霍志英)[4], Hua-Wei Zhang (张华伟)[1,3], Mao-Sheng Xiang (向茂盛),[4], Hai-Bo Yuan (苑海波)[5], Yang Huang (黄样)[2], Chun Wang (王春)[1,2] and Xiao-Wei Liu (刘晓为)[2]

[1] Department of Astronomy, Peking University, Beijing 100871, China; *zhanghw@pku.edu.cn*
[2] South-Western Institute for Astronomy Research, Yunnan University, Kunming 650500, China; *x.liu@ynu.edu.cn, bchen@ynu.edu.cn*
[3] Kavli Institute for Astronomy and Astrophysics, Peking University, Beijing 100871, China
[4] National Astronomical Observatories, Chinese Academy of Sciences, Beijing 100101, China
[5] Department of Astronomy, Beijing Normal University, Beijing 100875, China

Abstract We present a catalogue of 3305 Hα emission-line point sources observed with the Large Sky Area Multi-Object Fiber Spectroscopic Telescope (LAMOST) in the vicinity fields of M 31 and M 33 during September 2011 and January 2016. The catalogue contains 1487 emission-line stars, 532 emission-line nebulae including 377 likely planetary nebulae (PNe), 83 H II region candidates and 20 possible supernova remnants (SNRs) and 1286 unknown objects. Among them, 24 PN candidates, 19 H II region candidates, 10 SNR candidates and one symbiotic star candidate are new discoveries. Radial velocities and fluxes estimated from the Hα line and those quantities of seven other major emission lines including Hβ, [O III] λ4959, [O III] λ5007, [N II] λ6548, [N II] λ6583, [S II] λ6717 and [S II] λ6731 lines of all the catalogued sources yielded from the LAMOST spectra are also presented in our catalogue. Our catalogue is an ideal starting point to study the chemistry properties and kinematics of M 31 and M 33.

Key words: galaxies: individual (M 31, M 33) — stars: emission-line — planetary nebulae: general — H II regions

1 INTRODUCTION

The Andromeda Galaxy (M 31), the closest spiral galaxy and the most dominant member of the Local Group, is always one of the most interesting targets for astronomers. The Triangulum Galaxy (M 33), located in the southeast of M 31 (about 15° away), is the third most massive member in the Local Group. A large number of works have been carried out to investigate the properties and to conjecture the accretion and evolution history of the stellar substructures and dwarf galaxies in the halo of M 31 and M 33 in recent years (e.g., Ibata et al. 2001; Ferguson et al. 2002; Kalirai et al. 2006; Gilbert et al. 2007; Ibata et al. 2007; Gilbert et al. 2009; McConnachie et al. 2009; Tanaka et al. 2010 and references therein). Most of these studies are based on the photometric data. Due to the large distances of M 31 and M 33 (783 ± 25 kpc for M 31 and 809 ± 24 kpc for

M 33; McConnachie et al. 2005), it is challenging for the present ground and space telescopes to give spectroscopic observations for the individual M 31 and M 33 objects, except for some very bright objects, such as the globular clusters and emission-line sources including the planetary nebulae (PNe) and H II regions. The emission-line objects, whose energies are concentrated on a few emission lines, are excellent tracers for the study of the kinematics and chemistry properties of their host galaxies.

Many efforts have been made to identify and study the emission-line objects in M 31 and M 33. More than 30 years ago, Nolthenius & Ford (1984) have identified 34 PNe in M 31. Merrett et al. (2006) have presented a catalogue of 3300 emission-line objects in the M 31 area from the Planetary Nebular Spectrograph Survey. 2730 of them are likely PNe, including 2615 objects belonging to M 31 and the remaining objects associating with the

satellite galaxies and substructures of M 31. Azimlu et al. (2011) have presented a catalogue of 3691 H II regions in M 31 from the observations by the Mosaic Camera of the Mayall telescope and investigated the Hα luminosity function of M 31. Sanders et al. (2012) have studied the metallicity profile of M 31 based on the spectra of hundreds of H II regions and PNe observed by the Multiple Mirror Telescope (MMT). Lin et al. (2017) have observed 413 H II regions in M 33 with MMT and analyzed the detail temperatures and oxygen abundances distributions of M 33. Martin et al. (2018) have presented a catalogue of about 800 emission-line point-like sources in the central region of M 31 based on the observation from Canada-France-Hawaii Telescope. Li et al. (2018) obtained optical spectra of 77 PNe in the circumnuclear region of M 31 using the WIYN/Hydra multi-fiber spectrograph.

With 4000 fibers in a field of view of $20 \deg^2$, the Large Sky Area Multi-Object Fiber Spectroscopic Telescope (LAMOST; Cui et al. 2004) is a powerful facility to archive spectra of millions of detectable objects. As an extension part of the LAMOST Spectroscopic Survey of the Galactic Anti-center (LSS-GAC; Liu et al. 2014; Yuan et al. 2015), the LAMOST M 31/M 33 survey targets interesting objects in the vicinity fields of M 31 and M 33, including the detectable objects in M 31 and M 33, such as the supergiants, PNe (Yuan et al. 2010; Xiang et al. 2017) , H II regions and globular clusters (Chen et al. 2015, 2016), background quasars (Huo et al. 2010, 2013, 2015) and foreground Galactic stars.

In this paper, we will present a systematic search of the Hα emission-line point sources in the vicinity fields of M 31 and M 33, based on the LAMOST M 31/M 33 survey data observed during October 2011 and January 2016.

The paper is organized as follows. In Section 2, we briefly introduce the LAMOST observation and data reduction. Section 3 shows the selection of the Hα emission-line point sources and Section 4 gives the results. Finally we summarize in Section 5.

2 LAMOST OBSERVATION AND DATA REDUCTION

Objects targeted by LAMOST in the M 31 and M 33 region include known and candidate objects in M 31 and M 33, such as PNe, supergiants, H II regions and globular clusters, known and candidate background quasars, and foreground Galactic stars. An overview of the target selection of the LAMOST M 31/M 33 survey can be referred to Yuan et al. (2015). The LAMOST M 31/M 33 survey are targeted by LAMOST telescope from September to January of the next year in each observational season. The typical total exposure time, depending on the weather conditions, are 600–1200 s, 1200–1800 s and 1800–2400 s for bright (B),

medium (M) and faint (F) plates, respectively. For most plates, the seeing varies between 3 and 4 arcsec, with a typical value of about 3.5 arcsec (Yuan et al. 2015).

This work is based on spectra observed by LAMOST during September 2011 and January 2016. In total, 1 114 164 spectra have been collected by the LAMOST M 31/M 33 survey. Raw data was reduced by the LAMOST two-dimensional (2D) pipeline (Luo et al. 2015), including procedures of bias subtraction, cosmic ray removal, 1D spectral extraction, flat field correction, wavelength calibration and sky subtraction. The LAMOST spectra are separately recorded in blue (3700–5900 Å) and red (5700–9000 Å) arms. The blue and red spectra are processed by the 2D pipeline independently and combined together after the flux calibration, which is processed by an algorithm specifically designed for the LSS-GAC survey (Xiang et al. 2015). The final combined 1D spectra are then adopted to search for the Hα emission-line objects and to obtain their properties in this work.

3 SELECTIONS OF Hα EMISSION-LINE POINT SOURCES

We first select objects with spectra that have Hα emission-line by the criteria of signal-to-noise ratio in the wavelength of 6563 Å larger than 5. This yields a sample of 23 976 Hα emission-line candidates. Their Hα line profiles are then fitted by Gaussian functions and checked by naked eyes. Any bad spectrum that has poor flat-fielding or sky subtraction is then excluded. As a result, this yields 4448 unique objects as Hα line emission-line sources. Figure 1 shows an example of the Gaussian fitting of the Hα emission line for an example object.

In the current work, we are only interested in the Hα emission-line point sources. To exclude the extended sources such as the background galaxies and dwarf galaxies from our sample, we adopt the images and photometric catalogue of the Panoramic Survey Telescope and Rapid Response System-1 (Pan-STARRS 1; Kaiser et al. 2002, 2010). 795 candidates that are flagged as extended sources in the Pan-STARRS 1 catalogue are first excluded in our sample. The Pan-STARRS 1 r-band images of all the remaining objects are visually examined to make sure that all sources in our sample are point sources and free from any contaminators.

There are usually two to three singular explosions for each LAMOST observation. Finally, we have visually examined the singular exposure spectra of the remaining sources and remove objects with fake Hα emission line which appear in only one of those singular explosion spectra. As a result, we obtain 3305 unique Hα emission-line point sources as our final sample.
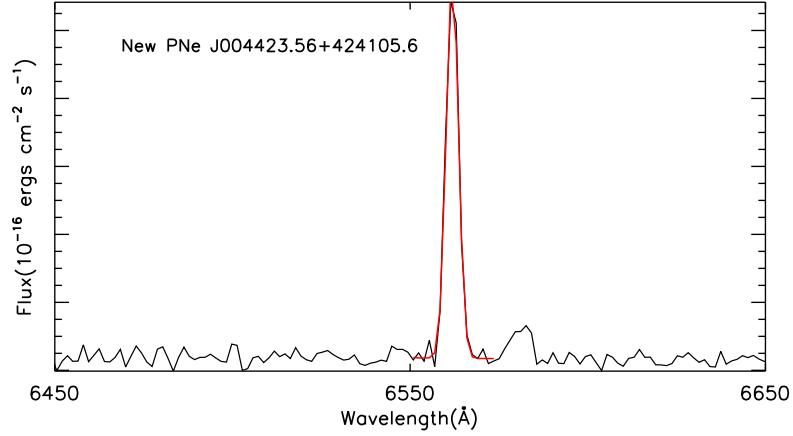
Fig. 1 The Gaussian fitting of the Hα emission line for object J00423.56+424105.6. The *black* and *red lines* show the LAMOST spectrum and the fitting results, respectively.

Table 1 Description of the Catalogue

Column	Name	Description
1	ID	Object ID
2	name	Object name
3	RA	Right Ascension (J2000)
4	Dec	Declination (J2000)
5	plate	LAMOST Plate ID
6	spid	LAMOST Spectrograph ID
7	fbid	LAMOST Fiber ID
8	mjd	Observed MJD
9	objtype	Object type tagged in the input catalogue
10	Vha	Radial velocity estimated from Hα line
11	Vhaerr	Uncertainty of radial velocity estimated from Hα line
12	fluxha	Flux of Hα line
13	fluxhaerr	Uncertainty of flux of Hα line
14	Vhb	Radial velocity estimated from Hβ line
15	Vhberr	Uncertainty of radial velocity estimated from Hβ line
16	fluxhb	Flux of Hβ line
17	fluxhberr	Uncertainty of flux of Hβ line
18	V4959	Radial velocity estimated from [O III] λ4959 line
19	V4959err	Uncertainty of radial velocity estimated from [O III] λ4959 line
20	flux4959	Flux of [O III] λ4959 line
21	flux4959err	Uncertainty of flux of [O III] λ4959 line
22	V5007	Radial velocity estimated from [O III] λ5007 line
23	V5007err	Uncertainty of radial velocity estimated from[O III] λ5007 line
24	flux5007	Flux of [O III] λ5007 line
25	flux5007err	Uncertainty of flux of [O III] λ5007 line
26	V6548	Radial velocity estimated from [N II] λ6548 line
27	V6548err	Uncertainty of radial velocity estimated from [N II] λ6548 line
28	flux6548	Flux of [N II] λ6548 line
29	flux6548err	Uncertainty of flux of [N II] λ6548 line
30	V6583	Radial velocity estimated from [N II] λ6583 line
31	V6583err	Uncertainty of radial velocity estimated from [N II] λ6583 line
32	flux6583	Flux of [N II] λ6583 line
33	flux6583err	Uncertainty of flux of [N II] λ6583 line
34	V6717	Radial velocity estimated from [S II] λ6717 line
35	V6717err	Uncertainty of radial velocity estimated from [S II] λ6717 line
36	flux6717	Flux of [S II] λ6717 line
37	flux6717err	Uncertainty of flux of [S II] λ6717 line
38	V6731	Radial velocity estimated from [S II] λ6731 line
39	V6731err	Uncertainty of radial velocity estimated from [S II] λ6731 line
40	flux6731	Flux of [S II] λ6731 line
41	flux6731err	Uncertainty of flux of [S II] λ6731 line
42	type	Object classification of this work

Table 2 Summary of the Catalogue

	Type	Number
Emission stars	New symbiotic star candidate	1
	Others (M dwarfs and B[e] stars, etc.)	1486
Emission Nebulae	Literature PNe	353
	New PN candidates	24
	Literature H II regions	64
	New H II region candidates	19
	Literature SNRs	10
	New SNR candidates	10
	Objects with [O III] λ5007 flux < 3	52
Others	Galaxies and unknown objects	1286
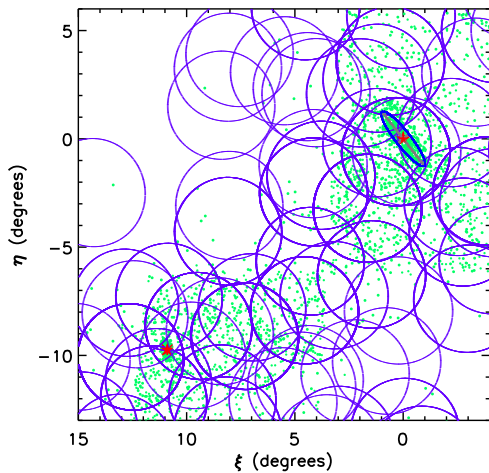
Fig. 2 Spatial distributions of Hα emission-line point sources in the vicinity fields of M 31 and M 33. The *purple circles* mark the LAMOST plates. The *red stars* show the center of M 31 and M 33, respectively. The *blue elliptic* with a semi-major radius of 95.3 arcmin marks the disk region of M 31.

4 RESULTS

Our catalogue is available in electronic form in the online version of this manuscript. Table 1 describes the data format of the catalogue. Each row of the catalogue contains the ID, name, coordinates and LAMOST observational information, such as the Plate ID, Spectrograph ID, Fiber ID, observed MJD and the object type tagged in the input catalogue, of the catalogued objects. Multiple observations of the same object are listed together with the same ID and object name. Figure 2 shows the spatial distribution of all the catalogued Hα emission-line point sources in the vicinity fields of M 31 and M 33 in the ξ–η plane. Here ξ and η are respectively the right ascension and declination offsets relative to the optical center of M 31.

For all the catalogued objects, we have made Gaussian fits to their Hα emission lines. If there are other prominent emission lines such as Hβ, [O III] λ4959, [O III] λ5007, [N II] λ6548, [N II] λ6583, [S II] λ6717 and [S II] λ6731 lines in the spectra, the Gaussian profile fits are also ap-

plied to these lines. Some of the emission lines (e.g., Hα and [N II] λ6583 lines) are located in narrow wavelength ranges. In those cases, the spectra are fitted by multiple Gaussian profiles, with one Gaussian component corresponding to one emission line. The center wavelength and integrated area of the Gaussian profiles define the radial velocities and fluxes of the corresponding lines. The resulted properties such as the radial velocity and flux of the Hα and seven other prominent emission lines (Hβ, [O III] λ4959, [O III] λ5007, [N II] λ6548, [N II] λ6583, [S II] λ6717 and [S II] λ6731) are also listed in our catalogue.

There are 745 duplicate observations for our catalogued objects. In Figure 3 we show the distribution of the differences of radial velocities from the Hα line deduced from the duplicate observations. The rms of the differences is about $15 \, \mathrm{km \, s^{-1}}$, which indicate a internal uncertainty of about $10 \, \mathrm{km \, s^{-1}}$ for the Hα line radial velocities.

Our Hα emission-line point source catalogue consists of objects of different types, including the emission-line object such as PNe, H II regions and supernova remnants (SNRs) in M 31 and M 33 and the Galactic emission-line stars. We cross-match our sample with the SIMBAD Astronomical Database and find 575 of them been classified, including 213 PNe, 161 emission-line stars and some other types of objects such as H II regions and SNRs. However, as some of the SIMBAD sources are identified by only photometric data. Their classification would be incorrect. In the current work, we will provide new classifications to the catalogued objects based on information of the LAMOST spectroscopic observations. The new classifications are also listed in the catalogue and a summary is given in Table 2.

4.1 Emission-Line Stars

Based on their LAMOST spectra, the catalogued objects can be roughly divided into two groups, one group of objects with significant continuum spectrum and the other group without. There are 1487 objects in our catalogue belonging to the first group. Most of them have spectra of typical stars and have only the Hα emission lines. We clas-
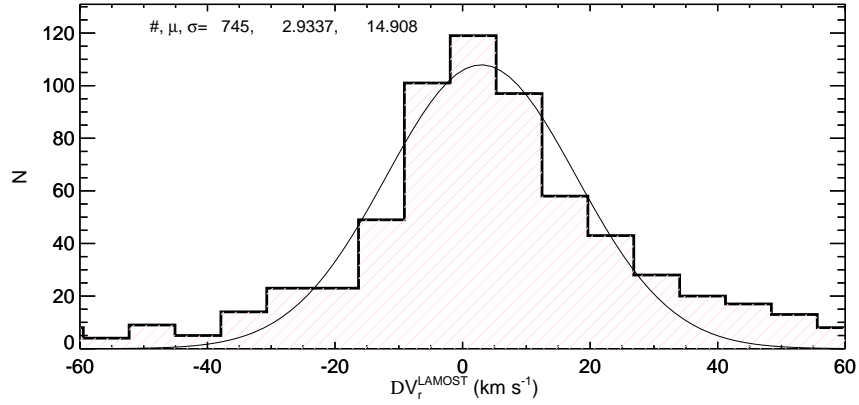
Fig. 3 Histogram of the differences of radial velocities from Hα line deduced from duplicate observations of the same targets. A Gaussian fit to the distribution is overplotted, with the number of objects with duplicate observations, and the mean and dispersion of the Gaussian marked.
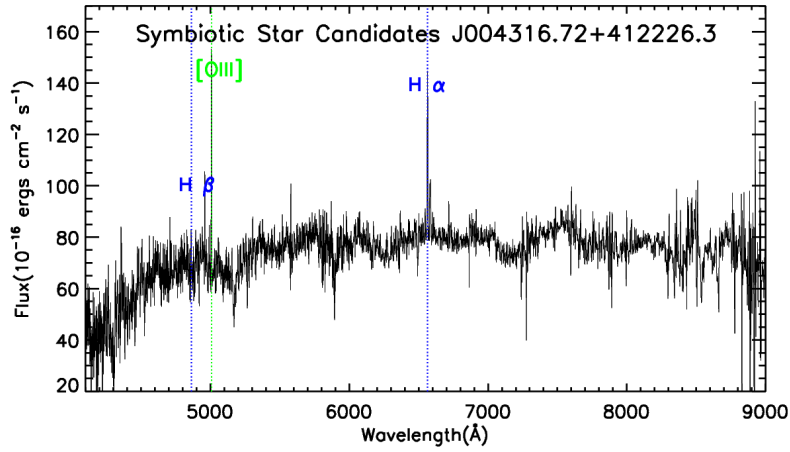

Fig. 4 LAMOST spectrum of a possible symbiotic star LAMOST J004316.72+412226.3. *Vertical lines with different colors* mark the positions of the different emission lines.
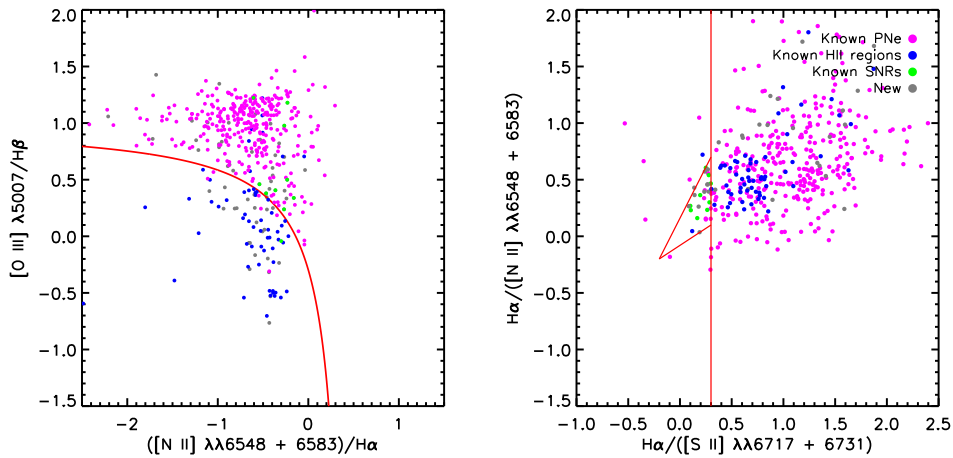

Fig. 5 The BPT (*left*) and SMB (*right*) diagrams of our catalogued emission-line nebulae with strong [O III] λ5007 emission (*grey dots*). Known PNe, H II regions and SNRs are plotted as *pink*, *blue* and *green dots*, respectively. The *red line* in the left panel marks the line we adopted to separate PNe and H II regions while those in the right panel are the criterion we adopted to select the SNR candidates (see text for details).
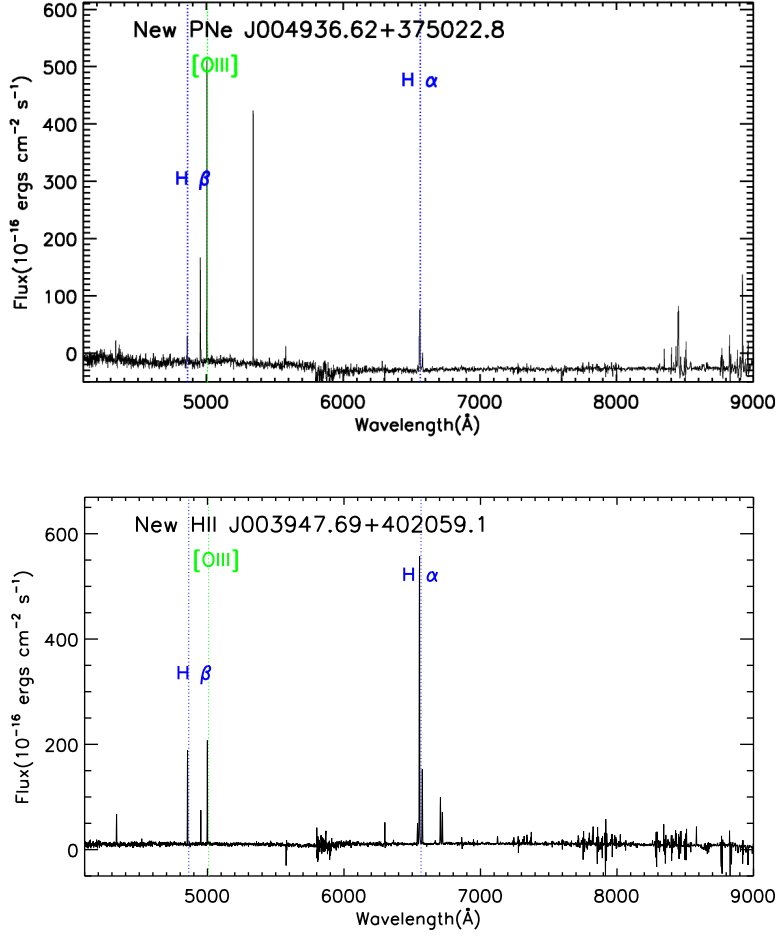
Fig. 6 LAMOST spectra of a PN candidate LAMOST J004936.62+375022.8 (upper panel) and a H II region candidate LAMOST J003947.69+402059.1 (bottom panel). *Vertical lines with different colors* mark the positions of the different emission lines.

sify them as emission-line stars in the current work. Most of the emission-line stars are M dwarfs displaying strong TiO bands. There are also several B[e] stars, which are B-type main-sequence sub-giant or giant stars with prominent Balmer emission, and some novae.

One of our catalogued object, LAMOST J004316.72 + 412226.3, has a spectrum that is very likely to be a symbiotic star. Symbiotic stars are interacting binaries which usually contain a white dwarf and a red giant (Mikołajewska et al. 2014). The spectrum of a symbiotic star usually presents both the feature of a late-type M giant and strong emission lines such as the Balmer H I lines and the [O III] λ5007 forbidden lines. The possible symbiotic star LAMOST J004316.72+412226.3 we find in the current work was classified as a PN in Halliday et al. (2006). Its LAMOST spectrum is displayed in Figure 4. The spectrum shows typical features of M stars in the red band and hot stars in the blue band. The emission lines of Hα and [O III] λ5007 lines are significant. However, due to the low resolution and limited signal-to-noise ratio of the

LAMOST spectrum, follow up observations of this object are needed for any further confirmation.

4.2 Emission-Line Nebulae

In our catalogue, there are 532 objects which display no obvious continuum spectra but have abundant emission lines. They are possible PNe, H II regions, and SNRs.

To exclude the contamination of early type stars, in the current work, we classify only the sources with strong emission of [O III] λ5007 line. These are objects of high electron excitation states, i.e., PNe, H II regions and SNRs. In the current work, we have selected 480 sources with [O III] λ5007 fluxes greater than 3. To distinguish the PNe, H II regions and SNRs from each others, we adopt the commonly used "Baldwin, Phillips & Terlevich" (BPT) and "Sabbadin, Minello & Biancini" (SMB) diagrams. The BPT diagram, which demonstrate how PNe can be distinguished from H II regions on the basis of their [O III] λ5007/Hβ (noted as 'O3') and ([N II] $\lambda\lambda$6548 +

6583)/Hα (noted as 'N2') flux ratios (Baldwin et al. 1981), is then adopted to classify the PNe and H II region candidates in our catalogue. Comparing to PN and H II region, the sulfur in SNR is usually found in a wide range of ionization states and the nitrogen emission line of SNR is sensitive to the presence of its radiative shock. We thus adopt the SMB diagram which separate the SNRs from PNe and H II regions by Hα/([N II] λλ6548 + 6583) (noted as 'n2') and Hα/([S II] λλ6717 + 6731) (noted as 's2') flux ratios (Sabbadin et al. 1977; Canto 1981 and Riesgo & López 2006). Figure 5 shows the BPT and SMB diagrams of our catalogued emission-line nebulae with strong emission lines of [O III] λ5007. As a result, we have identified 377 likely PNe, 83 possible H II regions and 20 SNRs candidates in our catalogue.
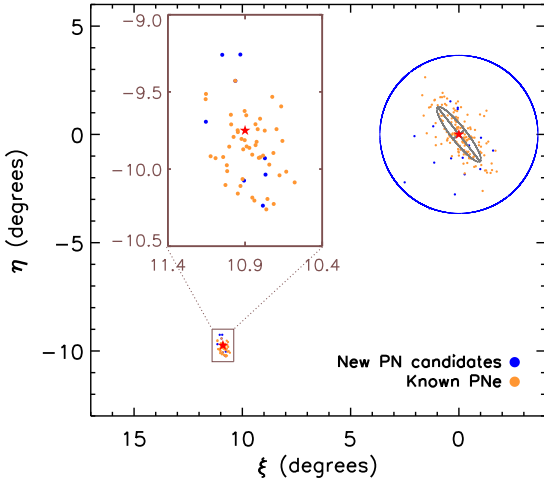

Fig. 7 The spatial distribution of the new PN candidates (*blue dots*) and known PNe from SIMBAD (*orange dots*) in our catalogue. *Red star symbols* mark the center of the M 31 and M 33 and the *grey ellipse* the M 31 disk region with a semi-major radius of 95.3 arcmin. The *blue circle* shows the region with a projected distance of 50 kpc to the M 31 center.

4.2.1 Planetary nebulae

The curve O3 > 0.61/(N2 − 0.47) + 1.0 (Sanders et al. 2012) separates the PNe and H II regions nicely (Fig. 5). It is adopted in the current work to select the PNe and we have identified 377 PN candidates in our catalogue, including 353 known PNe from the literature and 24 new discoveries. The spectrum of an example PN candidate is shown in Figure 6. The spatial distribution of all the PN candidates is shown in Figure 7. Most of the PN candidates are distributed in the disk regions of M 31 and M 33. However, some of the PN candidates, especially those newly discovered ones, are located in the halo regions of M 31 and M 33. They are valuable for us to study the chemistry and kine-
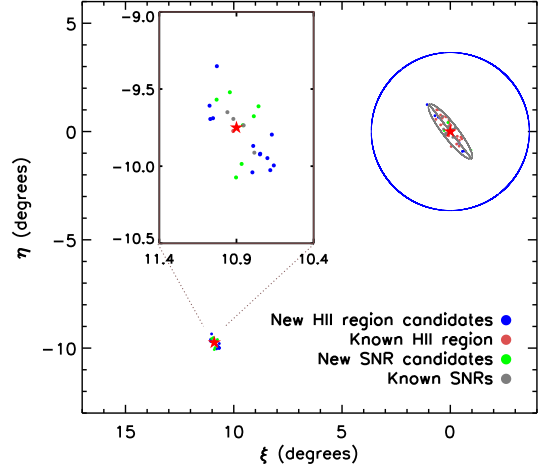

Fig. 8 Similar as Fig. 7 but for H II regions and SNRs. Known and newly identified candidate H II regions, as well as known and new SNR candidates are plotted with *brown*, *blue, grey* and *green dots*, respectively.

matics of the halos of M 31 and M 33 as well as streams in the halos.

4.2.2 H II regions

From the BPT diagram, we have identified 83 H II region candidates in our catalogue, including 64 known objects from the literature and 19 new identifications. The LAMOST spectrum of an example H II region candidate is also shown in Figure 6 and the spatial distribution of all the catalogued H II region candidates is shown in Figure 8.

4.2.3 Supernova remnants

Following the work of Frew et al.(2010), we adopt criteria: $0.6 \log s2 − 0.08 < \log n2 < 1.8 \log s2 + 0.16$ and $\log n2 < 0.3$ to select the SNR candidates (Fig. 5). As a result, we have identified 20 SNR candidates in the current work, including 10 known ones from literature and 10 new discoveries. Their spatial distribution is also shown in Figure 8.

5 SUMMARY

Based on the spectroscopic data from LAMOST M 31/M 33 survey during September, 2011 and June, 2016, we have selected 3305 Hα emission-line point sources in the vicinity of M 31 and M 33. We have calculated radial velocities and fluxes of Hα line and those quantities of other seven major emission lines (Hβ, [O III] λ4959, [O III] λ5007, [N II] λ6548, [N II] λ6583, [S II] λ6717 and [S II] λ6731) of all these catalogued sources from their LAMOST spectra by Gaussian profile

fitting method. In our catalogue, we have identified 1487 emission-line stars, including one new symbiotic star candidate, 532 emission-line nebulae, including 24 new PN candidates, 19 new H II region candidates and 10 new SNR candidates, and 1286 unknown objects. Our catalogue is available in electronic form in the online version of this manuscript. It will serve as an ideal starting point to study the chemistry properties and kinematics of the M 31.

References

Azimlu, M., Marciniak, R., & Barmby, P. 2011, AJ, 142, 139

Baldwin, J. A., Phillips, M. M., & Terlevich, R. 1981, PASP, 93, 5

Canto, J. 1981, in Astrophysics and Space Science Library, 91, Investigating the Universe, ed. F. D. Kahn, 95

Chen, B.-Q., Liu, X.-W., Xiang, M.-S., et al. 2015, RAA (Research in Astronomy and Astrophysics), 15, 1392

Chen, B., Liu, X., Xiang, M., et al. 2016, AJ, 152, 45

Cui, X., Su, D., Li, G., et al. 2004, in Society of Photo-Optical Instrumentation Engineers (SPIE) Conference Series, 5489, Experiment System of LAMOST Active Optics, eds. J. Oschmann, & Jacobus M., 974

Ferguson, A. M. N., Irwin, M. J., Ibata, R. A., Lewis, G. F., & Tanvir, N. R. 2002, AJ, 124, 1452

Frew, D. J., & Parker, Q. A. 2010, PASA, 27, 129

Gilbert, K. M., Fardal, M., Kalirai, J. S., et al. 2007, ApJ, 668, 245

Gilbert, K. M., Guhathakurta, P., Kollipara, P., et al. 2009, ApJ, 705, 1275

Halliday, C., Carter, D., Bridges, T. J., et al. 2006, MNRAS, 369, 97

Huo, Z.-Y., Liu, X.-W., Yuan, H.-B., et al. 2010, RAA (Research in Astronomy and Astrophysics), 10, 612

Huo, Z.-Y., Liu, X.-W., Xiang, M.-S., et al. 2013, AJ, 145, 159

Huo, Z.-Y., Liu, X.-W., Xiang, M.-S., et al. 2015, RAA (Research in Astronomy and Astrophysics), 15, 1438

Ibata, R., Irwin, M., Lewis, G., Ferguson, A. M. N., & Tanvir, N. 2001, Nature, 412, 49

Ibata, R., Martin, N. F., Irwin, M., et al. 2007, ApJ, 671, 1591

Kaiser, N., Aussel, H., Burke, B. E., et al. 2002, in Society of Photo-Optical Instrumentation Engineers (SPIE) Conference Series, 4836, Pan-STARRS: A Large Synoptic Survey Telescope Array, eds. J. A. Tyson, & S. Wolff, 154

Kaiser, N., Burgett, W., Chambers, K., et al. 2010, in Proc. SPIE, 7733, Ground-based and Airborne Telescopes III, 77330E

Kalirai, J. S., Gilbert, K. M., Guhathakurta, P., et al. 2006, ApJ, 648, 389

Li, A.-Q., Li, Z.-Y., Dong, H., Fang, X., & Xu, X.-J. 2018, RAA (Research in Astronomy and Astrophysics), 18, 140

Lin, Z., Hu, N., Kong, X., et al. 2017, ApJ, 842, 97

Liu, X. W., Yuan, H. B., Huo, Z. Y., et al. 2014, in IAU Symposium, 298, Setting the Scene for Gaia and LAMOST, eds. S. Feltzing, G. Zhao, N. A. Walton, & P. Whitelock, 310

Luo, A. L., Zhao, Y.-H., Zhao, G., et al. 2015, RAA (Research in Astronomy and Astrophysics), 15, 1095

Martin, T. B., Drissen, L., & Melchior, A.-L. 2018, MNRAS, 473, 4130

McConnachie, A. W., Irwin, M. J., Ferguson, A. M. N., et al. 2005, MNRAS, 356, 979

McConnachie, A. W., Irwin, M. J., Ibata, R. A., et al. 2009, Nature, 461, 66

Merrett, H. R., Merrifield, M. R., Douglas, N. G., et al. 2006, MNRAS, 369, 120

Mikołajewska, J., Caldwell, N., & Shara, M. M. 2014, MNRAS, 444, 586

Nolthenius, R. A. 1984, The Distribution and Dynamics of Planetary Nebulae in M32 and the Andromeda Galaxy, PhD Thesis, California Univ., Los Angeles

Riesgo, H., & López, J. A. 2006, RMxAA, 42, 47

Sabbadin, F., Minello, S., & Bianchini, A. 1977, A&A, 60, 147

Sanders, N. E., Caldwell, N., McDowell, J., & Harding, P. 2012, ApJ, 758, 133

Tanaka, M., Chiba, M., Komiyama, Y., et al. 2010, ApJ, 708, 1168

Xiang, M., Liu, X., Zhang, M., Yuan, H., & Huo, Z. 2017, in IAU Symposium, 323, Planetary Nebulae: Multi-Wavelength Probes of Stellar and Galactic Evolution, eds. X. Liu, L. Stanghellini, & A. Karakas, 388

Xiang, M. S., Liu, X. W., Yuan, H. B., et al. 2015, MNRAS, 448, 822

Yuan, H.-B., Liu, X.-W., Huo, Z.-Y., et al. 2010, RAA (Research in Astronomy and Astrophysics), 10, 599

Yuan, H. B., Liu, X. W., Huo, Z. Y., et al. 2015, MNRAS, 448, 855